DIRECT FLOW SIMULATIONS OF THIXOTROPIC LIQUIDS IN AGITATED TANKS

J. J. Derksen*

Chemical & Materials Engineering Department, University of Alberta, Edmonton, Alberta, Canada T6G 2G6

Simulations of transitional and turbulent flows of purely viscous thixotropic liquids in stirred tanks have been performed. The simple thixotropy model employed is based on the notion of a network in the liquid with an integrity that builds up with finite rate under quiescent conditions and breaks down under liquid deformation. We solve a transport equation for the network integrity which is two-way coupled to the lattice-Boltzmann-based flow solver. The liquid's time scale characterised by the dimensionless Deborah number demonstrates to have profound impact on the level of mobilisation and the flow patterns in the mixing tanks, especially if the time scale of the liquid is of the same order as the circulation time in the tank. It also is shown to what extent increasing the impeller speed improves mobilisation.

On a effectué des simulations de courants transitoires et turbulents de liquides thixotropes purement visqueux dans des cuves à agitation. Le modèle thixotrope simple employé est fondé sur la notion d'un réseau dans le liquide avec une intégrité qui s'accumule à un taux fini dans des conditions quiescentes et se décompose lors d'une déformation liquide. Nous avons résolu une équation de transport pour l'intégrité du réseau qui est couplée de façon bidirectionnelle au résolveur de flux fondé sur Lattice Boltzmann. L'échelle de temps du liquide caractérisée par le nombre de Deborah sans dimension démontre une incidence profonde sur le degré de mobilisation et les modèles de courant dans les cuves de mélange, surtout si l'échelle de temps du liquide est du même ordre que le temps de circulation dans la cuve. On démontre également dans quelle mesure la vitesse de l'impulseur améliore la mobilisation.

Keywords: thixotropy, direct numerical simulation, mixing, stirred tanks, complex fluids

INTRODUCTION

Mainly with applications in oil sands processing (Masliyah et al., 2004) in mind, we perform direct numerical simulations of thixotropic liquids in agitated tanks. The range of applications is, however, wider since also in food, pharmaceutical, paper-and-pulp, and polymer industries (Lucas et al., 2009) handling of thixotropic liquids is abundant. Thixotropic liquids show time-dependence, that is, their constitutive relations contain terms related to the liquid's deformation history. A typical (micro physical/chemical) source of thixotropy is the presence of a structural network in the fluid that forms as a result of long-range interactions between, for example, microscopic solid particles (clay particles) dispersed in it. A strongly developed network results in a liquid that is hard to deform (highly viscous) and/or has elastic properties. Liquid deformation tends to disintegrate the network. Since usually the rate at which the network disintegrates under deformation, and builds up at quiescent conditions is finite (e.g., due to transport limitations at the micro level), the liquid's history in terms of its (absence of) deformation impacts the local rheological behaviour, hence thixotropy.

In many cases agitation of thixotropic liquids in mixing tanks is done to mobilise the liquid by breaking the network. The extent to which this happens is an intricate interplay between time scales (of the liquid and of the agitation), liquid inertia (relative to viscous forces), and the geometrical layout of the tank. As in many more situations where interaction and competition of a multitude of phenomena govern process behaviour, numerical simulation is a versatile way to reveal the interactions and to gain insight in the relative importance of these phenomena as a function of process conditions.

In this paper we build upon a computational methodology for thixotropic liquid flow we recently developed and verified for a number of laminar flow benchmark cases (Derksen and Prashant, 2009). Its computational efficiency allows for fine grids so that

*Author to whom correspondence may be addressed.
E-mail address: jos@ualberta.ca
Can. J. Chem. Eng. 89:628–635, 2011

DOI 10.1002/cjce.20413
Published online 9 November 2010 in Wiley Online Library (wileyonlinelibrary.com).

direct simulations of transitional and mildly turbulent flows in mixing tanks are within reach. The focus of the present paper is on the application of the methodology to agitation for mobilising thixotropic liquids.

A relatively simple thixotropy model has been adopted and the liquids considered are purely viscous, that is, no visco-elastic effects have been incorporated. In spite of these limitations, the dimensionality of the parameter space is much larger than it would be with simpler (Newtonian) liquids. For this reason we primarily limit our study to the impact of the time scale related to network build-up in the liquid (relative to the flow time scales) on the level of mobilisation, and on the effect of the impeller speed. In order to relate to agitated flows of Newtonian liquids we chose a standard stirred tank geometry: a Rushton turbine revolving in a baffled tank.

Literature on turbulent and transitional agitation of non-Newtonian liquids is relatively scarce. There is significant research activity in the field of drag reduction (e.g., Brostow et al., 2007; Escudier et al., 2009). In terms of agitated flows the literature is mostly related to shear-thinning and/or Bingham liquids with a time-independent rheology (Elson et al., 1986; Elson, 1990; Amanullah et al., 1998; Arratia et al., 2006; Derksen, 2009). Stirring yield-stress liquids in mixing tanks usually results in the formation of a cavity around the impeller: liquid only gets agitated in a part of the tank volume around the impeller, and—as for thixotropic liquids—mobilisation is a key issue. Recently, agitation of thixotropic liquids was studied experimentally and computationally (Couerbea et al., 2008). One of the main findings of that study was that the level of realism of simulations would benefit from more refined models for fluid behaviour and their computationally efficient implementation in CFD codes.

This paper is organised in the following manner: First the liquid's rheological model is described. Then the flow geometry is introduced. Along with the liquid characteristics this allows us to define a set of dimensionless numbers that are the coordinates of the parameter space we will be partly exploring. The subsequent section briefly describes the numerical methodology (more details are in Derksen and Prashant, 2009). In presenting the results, the focus is on the level of mobilisation, and on the flow structures encountered. The final section summarises the results and gives the main conclusions.

THIXOTROPY MODEL

The thixotropy model we use is based on work that dates back to the late 1950s (Storey and Merrill, 1958; Moore, 1959). More recently it has been applied by Ferroir et al. (2004) in their analysis of particle sedimentation in clay suspensions. It has been placed in a larger context of thixotropy modelling in the review due to Mujumdar et al. (2002). In the purely viscous (i.e., non-elastic) model we keep track of a scalar λ that varies between 0 and 1 and indicates the integrity of a structural network in the liquid ($\lambda = 0$: no network; $\lambda = 1$: fully developed network). Its transport equation reads:

$$\frac{\partial \lambda}{\partial t} + u_i \frac{\partial \lambda}{\partial x_i} = -k_1 \dot{\gamma} \lambda + k_2 (1-\lambda) \tag{1}$$

(summation over repeated indices) with u_i the ith component of the fluid velocity vector, and $\dot{\gamma} = \sqrt{2 d_{ij} d_{ij}}$ a generalised deformation rate; $d_{ij} = (1/2)((\partial u_j/\partial x_i) + (\partial u_i/\partial x_j))$ is the rate of strain tensor. The first term on the right hand side of Equation (1) indicates breakdown of the network due to liquid deformation; the second term is responsible for build-up of the network with a time constant $(1/k_2)$ associated to it. The network integrity is fed back to the liquid flow by relating it to the apparent viscosity η_a. The simple model (Ferroir et al., 2004) used here adopts a linear relation:

$$\eta_a = \eta_\infty (1 + \alpha \lambda) \tag{2}$$

In a homogeneous shear field with shear rate $\dot{\gamma}$, the steady-state solution to Equation (1) reads:

$$\lambda_{ss} = \frac{k_2}{k_1 \dot{\gamma} + k_2} \tag{3}$$

The associated steady state viscosity is (combine Equations 2 and 3):

$$\eta_{ss} = \eta_\infty \left(1 + \alpha \frac{k_2}{k_1 \dot{\gamma} + k_2} \right) \tag{4}$$

The parameter η_∞ can thus be interpreted as the infinite shear viscosity. The zero-shear viscosity is $\eta_\infty(1+\alpha)$. A typical representation of the steady-state rheology (Equation 4) is given in Figure 1.

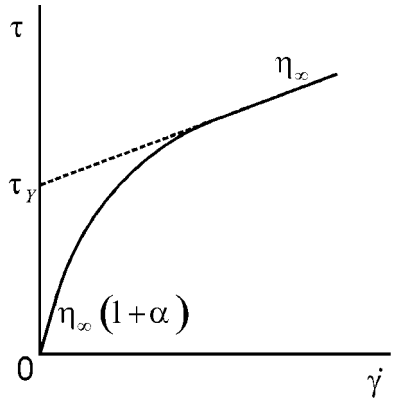

Figure 1. Steady-state rheology according to Equation (4). The infinite-shear viscosity is η_∞, the zero-shear viscosity is $\eta_\infty(1+\alpha)$. The pseudo yield stress τ_Y is defined by extrapolating the infinite shear behaviour towards $\dot{\gamma} = 0$.

The thixotropic liquid as defined by Equations (1) and (2) has four parameters: k_1, k_2, η_∞, α. This implies that once the flow geometry is defined, four dimensionless numbers are needed to fully pin down the flow conditions.

FLOW GEOMETRY

The baffled mixing tank is filled to a level $H = T$ (with T the tank diameter) with liquid, see Figure 2. A lid closes off the surface, that is, at the top a no-slip condition applies. Agitation is performed by a Rushton turbine, see Figure 2. A Rushton turbine has six short, vertical blades mounted on a disk. The disk is mounted on a shaft that enters from the top down to the level of the impeller. The primary flow induced by this impeller is in the radial direction. The Rushton turbine has a diameter equal to $D = T/3$. It rotates with an angular velocity of N revolutions per second. The choice of this standard impeller and tank configuration allows for relating the present simulations of thixotropic liquid flow with earlier works on Newtonian and also Bingham liquid flow in a similar geometry.

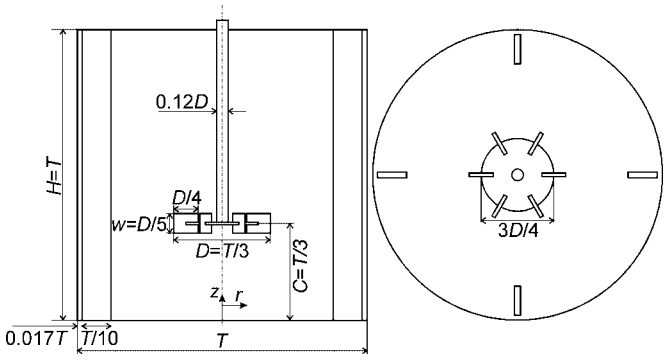

Figure 2. The stirred tank geometry considered in this paper: baffled tank with Rushton turbine (left: side view, right: top view). The (*r*, *z*) coordinate system has its origin in the centre at the bottom of the tank.

Now that we have defined the geometry, we can choose a set of four dimensionless numbers fully defining the flow of thixotropic liquid in the stirred tank. Three of the dimensionless numbers are straightforward: (1) a Reynolds number defined in the same way as traditionally done in Newtonian stirred tank flow but now with η_∞: $\mathrm{Re}_\infty = \rho N D^2/\eta_\infty$; (2) the ratio of zero-shear over infinite-shear viscosity $\alpha+1$; and (3) a time-scale ratio that we term Deborah number: $\mathrm{Db} = N/k_2$ (having a Deborah number does not mean we consider visco-elasticity). Db is the ratio of the time scale of the liquid divided by a macroscopic flow time scale for which we take the period of one impeller revolution ($1/N$). The choice of the fourth dimensionless number relates to the application perspective. If the rheogram in Figure 1 is interpreted as that of a (pseudo) Bingham liquid the intercept of the asymptote for high shear rates with the ordinate can be viewed as a pseudo yield stress: $\tau_\mathrm{Y} = \eta_\infty \alpha (k_2/k_1)$ (see Figure 1). The fourth dimensionless number then becomes a pseudo-Bingham number: $B_\mathrm{n} = (\tau_\mathrm{Y}/\eta_\infty N) = \alpha (k_2/k_1)(1/N)$. However, if the liquid is merely interpreted as shear thinning, the ratio k_2/k_1 can be viewed as the liquid's "characteristic" shear rate $\dot{\gamma}_\mathrm{c}$ (characteristic in the sense that the transition from zero-shear to infinite-shear viscosity takes place around $\dot{\gamma} = \dot{\gamma}_\mathrm{c}$, see Equation 4) and the dimensionless number would be typically chosen as $\dot{\gamma}_\mathrm{c}/N$. In this paper the Bingham liquid perspective will be taken, and the pseudo-Bingham number will be used so that the four dimensionless numbers are: Re_∞, α, Db, and B_n.

NUMERICAL APPROACH

The lattice-Boltzmann method (LBM) (Chen and Doolen, 1989; Succi, 2001; Yu et al., 2003) has been applied to numerically solve the incompressible flow equations. Lattice-Boltzmann fluids can be viewed as (fictitious) fluid particles moving over a regular lattice, and interacting with one another at lattice sites. These interactions (collisions) give rise to viscous behaviour of the fluid, just as colliding/interacting molecules do in real fluids. The main reasons for employing the LBM for fluid flow simulations are its computational efficiency and its inherent parallelism, both not being hampered by geometrical complexity.

In this paper the LBM formulation of Somers (1993) has been employed. It falls in the category of three-dimensional, 18 speed (D3Q18) models. Its grid is uniform and cubic. Planar, no-slip walls naturally follow when applying the bounce-back condition. For non-planar and/or moving walls (that we have in case we are simulating the flow in a cylindrical, baffled mixing tank with a revolving impeller) an adaptive force field technique (a.k.a. immersed boundary method) has been used (Goldstein et al., 1993; Derksen and Van den Akker, 1999).

To incorporate thixotropy, the viscosity needs to be made dependent on the local value of the network parameter λ (Equation 2), and (more importantly) the transport equation for the network parameter (Equation 1) needs to be solved. We solve Equation (1) with an explicit finite volume discretisation on the same (uniform and cubic) grid as the LBM. A clear advantage of employing a finite volume formulation is the availability of methods for suppressing numerical diffusion. This is particularly important in the present application since Equation (1) does not have a molecular or turbulent diffusion term; in order to correctly solve Equation (1) we cannot afford to have significant numerical diffusion. As in previous works (Hartmann et al., 2006; Derksen, 2008), TVD discretisation with the Superbee flux limiter for the convective fluxes (Sweby, 1984) was employed. We step in time according to an Euler explicit scheme with the source term (the right-hand-side of Equation 1) treated in an implicit manner to enhance stability (Derksen and Prashant, 2009).

DIMENSIONLESS AND NUMERICAL SETTINGS

The values for the infinite-shear viscosity η_∞ and the zero-shear viscosity $\eta_\infty(1+\alpha)$ were chosen such that the flow in the mixing tanks would be mildly turbulent if the liquid would be Newtonian with viscosity η_∞ (Re_∞ of the order of 10^4), and laminar with viscosity $\eta_\infty(1+\alpha)$ ($\mathrm{Re}_\infty/(1+\alpha) = O(10^2)$). With the lattice-Boltzmann flow solver (that enables the use of fine grids) in place, these Reynolds numbers allow for direct numerical simulations (DNS). This way we avoid the use of turbulence closure relations or subgrid-scale modelling. With DNS we fully resolve the (likely complex) interactions between liquid properties and flow structures, without having to consider potential artefacts related to turbulence modelling.

The tank to be simulated has lab-scale size with a tank volume of typically 10 L. A 10 L tank with a geometrical layout as given in Figure 2 has a diameter $T = 0.234$ m. The impeller diameter $D = T/3 = 0.078$ m. With a liquid having $\eta_\infty = 10^{-2}$ Pa s and $\rho = 10^3$ kg/m^3 we generate mildly turbulent flow if the impeller spins with $N = 10$ rev/s: $\mathrm{Re}_\infty = 6 \times 10^3$. Commonly used thixotropic liquids have time constants in the range of 0.1–10 s (see e.g., Dullaert and Mewis, 2005), so that the Deborah numbers fall in the range 1–100.

In this paper we only explore part of the four-dimensional parameter space as defined by the four dimensionless numbers Re_∞, Db, B_n, and $\alpha+1$. The viscosity ratio $\alpha+1$ has been set to a fixed value of 100. This way we ensure laminar flow if the network would be fully developed ($\lambda = 1$ everywhere). Three Deborah numbers will be considered: 1, 10, and 100. In addition, cases will be discussed where the liquid has a time-independent, shear thinning rheology according to Equation (4). Effectively this implies that the liquid adapts infinitely fast so that $1/k_2 \to 0$ and thus $\mathrm{Db} = 0$. For these four Db numbers, the base–case impeller speed has been chosen such that $\mathrm{Re}_\infty = 6 \times 10^3$, and $B_\mathrm{n} = 100$. Under these conditions (tank size, impeller speed, other liquid properties) $B_\mathrm{n} = 100$ corresponds to a (pseudo) yield stress of $\tau_\mathrm{Y} = 10$ N/m^2 which is a typical yield stress for the clay suspensions as encountered in oil sands waste stream processing. As we will see, under these base–case conditions the liquid sometimes gets only partially (and sometimes only marginally) mobilised. In order to check to what extent increasing the impeller speed helps in mobilising the liquid also higher impeller

speeds are investigated. At higher impeller speeds Re_∞ and Db increase, while B_n decreases.

In its basic implementation (as used in this study) the lattice-Boltzmann method applies a uniform, cubic grid. The spatial resolution of the grid was such that the tank diameter T equals 180 grid spacings Δ ($\Delta = T/180$). The time step is such that the impeller revolves once in 2000 time steps. The rotation of the impeller in the static grid is represented by an immersed boundary technique. In order to assess grid effects, a flow case was also simulated on a grid with resolution $\Delta = T/240$, and compared with its $T/180$ counterpart in terms of global time evolution of the structure parameter λ in the stirred tank.

As the default situation, the simulations were started with a zero liquid velocity field and a uniform network parameter $\lambda = 1$ (fully developed network). This mimics the common situation that the liquid has been standing still for sufficient time to develop a network after which we turn on the agitation to mobilise it. Our primary interests are in how the flow develops towards a (quasi) steady state, what flow structures can be observed in (quasi) steady state, and what the influence of the Deborah number and the impeller speed is on all this.

RESULTS

In order to assess how the flow in the tank evolves from a zero-velocity, fully networked ($\lambda = 1$) state towards a quasi steady, agitated state we show in Figure 3 time series of the tank-averaged network parameter $\langle\lambda\rangle$ for Db = 1, 10, and 100 (and further base–case conditions, $Re_\infty = 6 \times 10^3$, $B_n = 100$, $\alpha + 1 = 100$). Obviously agitation breaks down the network to a large extent. The time-scales of this process largely depend on the Deborah number; the slower the liquid, the slower the break-down process. For Db = 1 quasi steady state sets in after approximately 10 impeller revolutions, whereas it takes over 200 revolutions for Db = 100. At Db = 10 the route towards steady state is quite peculiar. After some 40 revolutions—when it looks like a steady state with $\langle\lambda\rangle \approx 0.33$ has been established—$\langle\lambda\rangle$ starts increasing slightly, however significantly with a final steady state that has $\langle\lambda\rangle \approx 0.39$ reached after slightly more than 100 impeller revolutions.

The evolution to steady state in terms of $\langle\lambda\rangle$ is quite insensitive with the grid resolution. In Figure 4 we show two cases (that for a change start with $\langle\lambda\rangle = 0$) that are the same in dimensionless terms, but that differ in grid spacing relative to tank diameter: $\Delta = T/180$ (default) and $\Delta = T/240$. As can be observed, the differences are small.

In order to interpret the evolution of the mobilisation process at Db = 10 (see Figure 3) in more detail, scalar distributions in the vertical, mid-baffle plane at various stages are given in Figure 5. The Rushton turbine first reduces the network parameter in its direct vicinity after which the breakdown process spreads

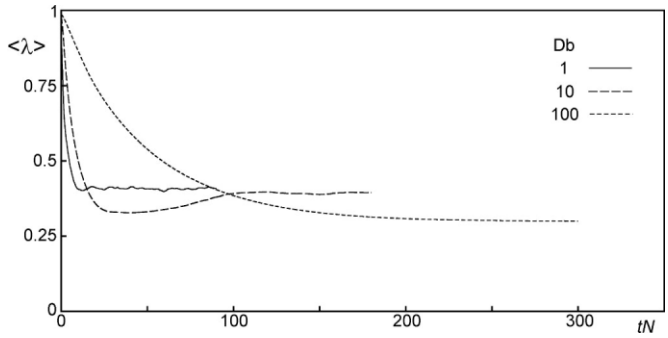

Figure 3. Time series of the tank average network parameter $\langle\lambda\rangle$ for three Deborah numbers as indicated.

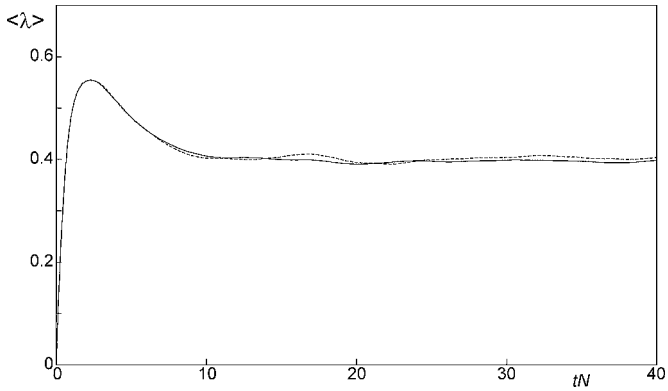

Figure 4. Time series of tank average network parameter $\langle\lambda\rangle$ for simulations with different spatial resolution. Dashed curves: $\Delta = T/180$; solid curves: $\Delta = T/240$. Re = 6000, Db = 1 starting from a zero flow field and $\lambda = 0$ everywhere.

throughout the tank. The slight increase of $\langle\lambda\rangle$ that sets in after 40 impeller revolutions as observed in Figure 3 is due to an intricate interplay between macro-scale flow and thixotropy effects. The strong radial stream emerging from the impeller and hitting the tank wall starts deflecting more and more downwards, thereby favouring the strength of the flow in the lower part of the tank, and weakening the flow in the upper part of the tank. This is a positive feedback process: It allows the network in the upper part of the tank to recover which further contributes to the downward deflection of the impeller stream and weakening the flow in the upper part even further. After roughly 100 revolutions the flow has settled in a state with strong flow in the volume below the impeller, and weak flow (and marginal mobilisation) in the volume above.

The Deborah number (and thus the time-dependent nature of the liquids) thus appears to be a crucial parameter for the level

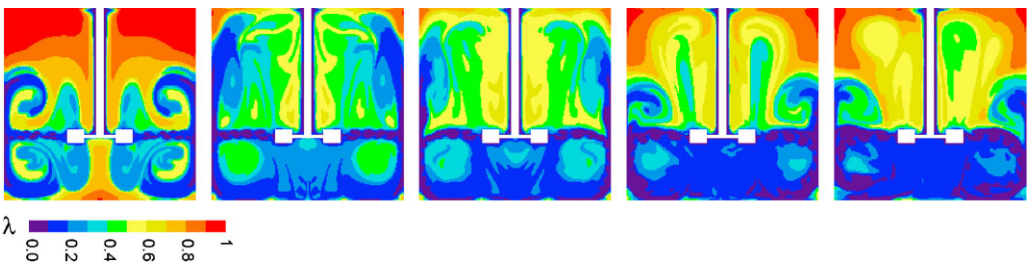

Figure 5. Instantaneous realisations of the λ-field in the vertical plane midway between baffles. Base–case with Db = 10. Flow at (from left to right) 10, 40, 70, 100, and 180 impeller revolutions after start-up.

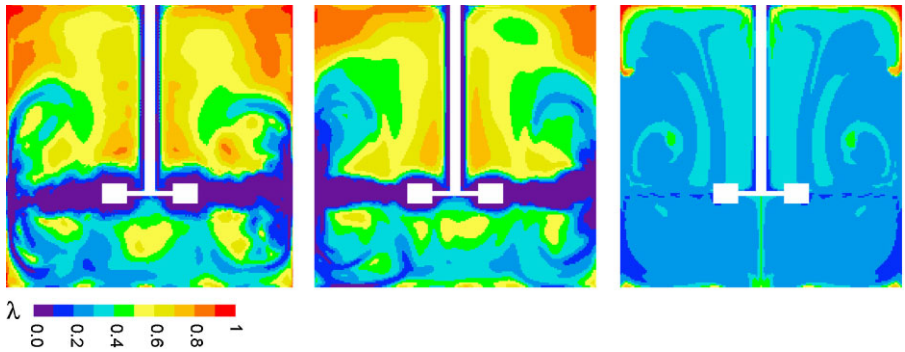

Figure 6. Instantaneous realisations of the λ-field in the vertical plane midway between baffles after quasi steady-state has been reached. From left to right: Db = 0, 1, and 100.

of mobilisation and (related) flow structures in the tank. It is worthwhile noting that under steady, homogeneous shear conditions the three liquids as used in Figure 3 display exactly the same shear-thinning behaviour (according to Equation 4). The lower the Deborah number, the faster the flow reaches (quasi) steady state, and also the higher the steady-state $\langle\lambda\rangle$. For low Deborah numbers, the liquid responds quickly to deformation (and absence of deformation). Therefore the regions in the liquid undergoing strong deformation due to agitation (notably the impeller-swept volume, and the impeller stream) largely overlap with regions of low λ. Given the liquid's quick response, the low-λ regions do not get a chance to be transported to the rest of the tank, leaving that part quite inactive (similar to cavern formation with Bingham liquids) and giving rise to relatively high tank-averaged network parameters. As we discussed above, the interactions between liquid and flow time scales give rise to a complex evolution of the flow for Db = 10. If Db increases further to 100, the delay between the moment the deformation is applied to the liquid and the destruction of the network increases, so that high deformation regions get dislocated from low viscosity regions. Similarly, more quiescent regions not necessarily get the change to develop high apparent viscosities. At Db = 100 the liquid is responding so slow that the network parameter λ gets fairly uniformly distributed in the tank.

In Figure 6 we show typical distributions of λ after quasi-steady state has been reached for Db = 0, 1, and 100. For Db = 0, the transport equation in λ (Equation 1) does not need to be solved; it can be determined directly from the local $\dot{\gamma}$ and Equation (3). Comparison of infinitely fast liquids (Db = 0) and time-dependent liquids agitated such that Db = 1 shows minor differences. This is further detailed in Figure 7 where we show axial profiles of the velocity fluctuation levels in terms of the turbulent kinetic energy k, and apparent viscosity η_a.

Apparently if the liquid is agitated such that Db = 1, the liquid's time dependence plays a minor role. At the other side of the spectrum, for large Db (Db = 100), λ gets (more or less) uniformly distributed throughout the tank. For the specific case considered here we expect laminar flow; the uniformity of λ results in a uniform and relatively high viscosity: in quasi steady state $\langle\lambda\rangle \approx 0.30$ so that $\langle\eta_a\rangle \approx 30\eta_\infty$ and $\langle \mathrm{Re}\rangle = \rho N D^2/\langle\eta_a\rangle \approx 200$.

For the λ-fields depicted in Figure 6 at Db = 1 and Db = 100, the corresponding velocity vector plots are given in Figure 8. At Db = 1 the impeller stream is transitional/turbulent whereas the flow in the rest of the tank is laminar. The placement of the impeller with a bottom clearance of $T/3$ makes the upper parts of the liquid virtually immobile. As expected, at Db = 100 the flow is laminar, however with a better overall mobility compared to the Db = 1 case.

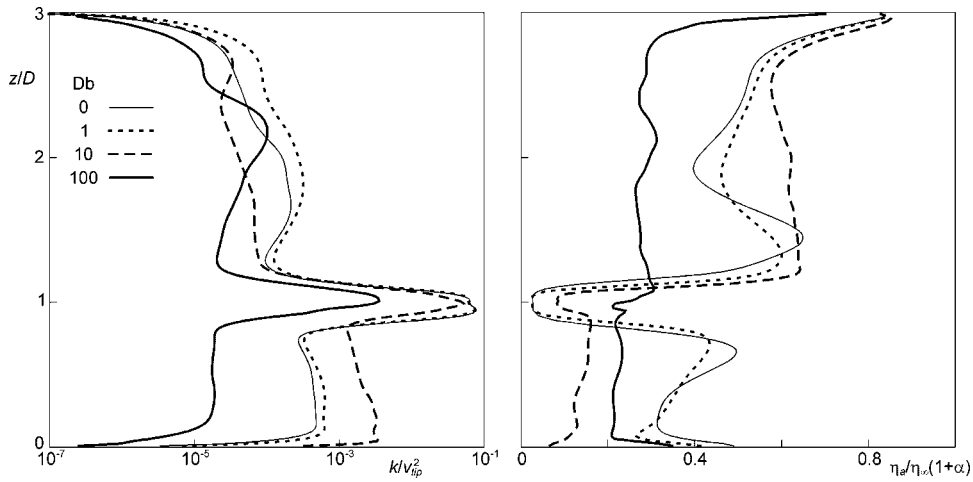

Figure 7. Vertical profiles at a radial position of $r = T/4$ of the time-average kinetic energy k, and the apparent viscosity η_a for the various Deborah numbers.

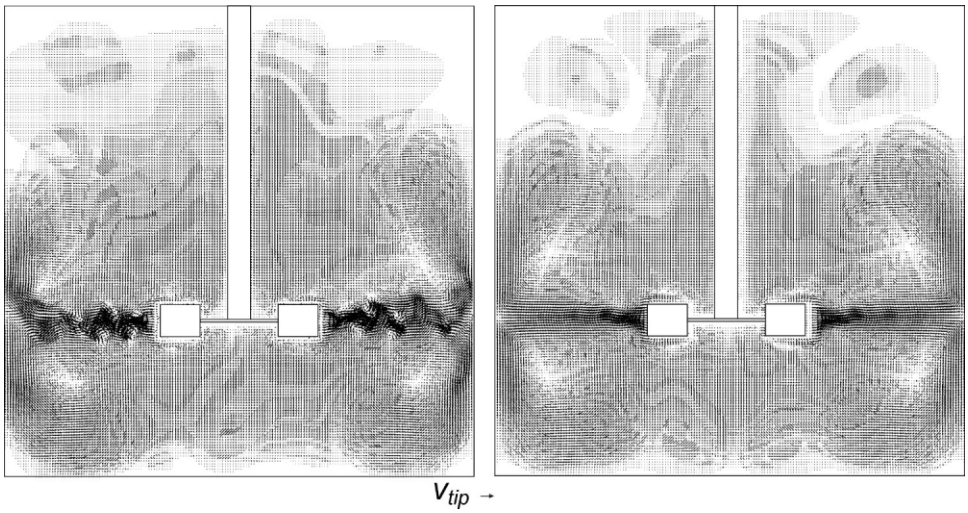

Figure 8. Snapshot of velocity vectors in the mid-baffle plane in the tank for Db = 1 (left) and Db = 100 (right) after quasi steady state has been reached.

An obvious way of enhancing liquid mobility is increasing the impeller speed N. Since changing N has consequences for three of the four dimensionless numbers that have been identified above we have chosen to present the simulation results directly as a function of the impeller speed relative to the base–case impeller speed (that gave rise to $\mathrm{Re}_\infty = 6 \times 10^3$, $B_\mathrm{n} = 100$). Slower liquids (liquids with higher Db-base values) benefit relatively more from increasing the impeller speed than faster liquids, especially in terms of the enhanced agitation mobilising bigger parts of the tank. This is illustrated in Figure 9. This figure shows λ contour plots for Db-base = 1, 10, and 100 at a three times higher impeller speed as compared to the base-speed.

SUMMARY

In this paper, a procedure for detailed simulations of flow of thixotropic liquids is applied to transitional and mildly turbulent agitated tank flow. Thixotropy is considered to be the result of the finite rate response of the integrity of a network in the liquid to local flow conditions. The thixotropy model used is very simple: It is purely viscous, it assumes linear relations for network build-up and breakdown (the latter due to deformation), and a linear relation between apparent viscosity and network integrity. This simple model, however, already comes with four parameters. Where single-phase mixing tank flow of Newtonian liquids can be captured by a single dimensionless number—the Reynolds number—(once the tank and impeller geometry in terms of aspect ratios has been defined, and if the tank does not have a free surface), we now need four dimensionless numbers to pin down the flow conditions. In this paper these dimensionless numbers are a Reynolds number Re_∞ based on the infinite-shear viscosity, a Deborah number Db being the time scale of the liquid relative to the time of a single impeller revolution, a pseudo-Bingham number B_n, and the ratio of zero-shear over infinite-shear viscosity. The aim of this paper is to see how thixotropy qualitatively impacts global flow structures and mixing and liquid mobilisation in agitated tanks. In our base–case simulations we fix the Reynolds number to $\mathrm{Re}_\infty = 6 \times 10^3$ which allows us to perform DNS, the Bingham number to $B_\mathrm{n} = 100$ which translates to a pseudo yield stress of order $10\,\mathrm{N/m^2}$ in our lab-scale (10 L) setups, and the viscosity ratio to 100.

The primary characteristic of thixotropy is the effect of the deformation history on the liquid's rheological behaviour. In terms of the dimensionless numbers considered here, thixotropic liquids give rise to non-zero Deborah number. For this reason we studied the effect the Deborah number has on the flow. Comparing flows with Db = 1 and Db = 0 only shows marginal differences which implies that the liquid's time dependence is not strongly

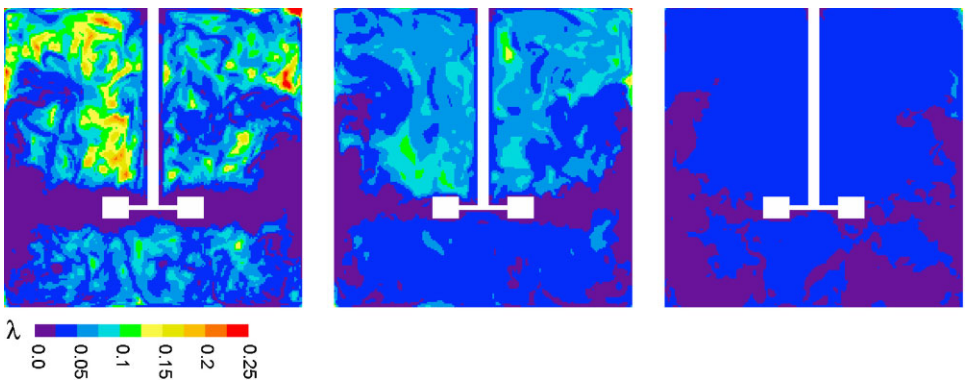

Figure 9. Snapshots of λ-contours for three times the base–case impeller speed. From left to right: Db-base = 1, 10, 100 respectively. Note the small high-λ spots in the upper corners of the right panel. Also note the different colour scale as compared to Figure 6.

felt if its time scale is of the order of the time required for one impeller revolution. At Db = 100, that is, at the other side of the Db-range considered, a slow evolution towards a fairly homogeneous distribution of the network parameter is observed resulting in—given the rest of the conditions—laminar flow. The uniformity is due to the large delay between deformation and network breakdown, and the slow build-up of the network under quiescent conditions. A more intriguing situation occurs when Db = 10. This case shows the strongest interaction between flow and liquid time scale, the reason probably being that the liquid time scale now gets comparable to the circulation time of the liquid in the tank (the flow number for a Rushton turbine is roughly equal to one which results in a circulation time of approximately $20/N$, see, e.g., Tiljander et al., 1997). The Rushton turbine flow at Db = 10 slowly (over some 100 revolutions) evolves to the undesired situation with strong flow underneath the impeller, and a largely immobile volume above.

Given the sometimes poorly mobilised tank volumes we subsequently studied to what extent increasing the impeller speed improves overall mobilisation. It does so in a manner that favours cases with high Deborah numbers.

The results presented in this paper are largely qualitative, and sensitive to the specific thixotropy model chosen. However, they do show a rich response of stirred tank flow to thixotropy. Furthermore, the methodology as outlined here is generic and can be easily adapted to more complicated (albeit viscous) rheological liquid descriptions. The method is computationally efficient (as demonstrated by the significant number of flow systems, and the significant numbers of impeller revolutions per flow system simulated) and geometrically flexible so that attacking practical mixing and mobilisation problems is within reach.

NOMENCLATURE

D	impeller diameter
d_{ij}	rate of strain tensor
k	turbulent kinetic energy
k_1, k_2	thixotropy parameters (Equation 1)
N	impeller angular velocity
r, z	radial and axial coordinate in tank (Figure 2)
T	tank diameter
t	time
u_i	fluid velocity component
v_{tip}	impeller tip speed
x_i	spatial coordinate
$\alpha + 1$	viscosity ratio
$\dot{\gamma}$, $\dot{\gamma}_c$	(characteristic) deformation rate
Δ	lattice spacing
η_a, η_∞	apparent, infinite-shear dynamic viscosity
λ, $\langle\lambda\rangle$	(tank-averaged) network integrity parameter
ρ	density
τ_Y	yield stress
B_n	Bingham number
Db	Deborah number
Re_∞	Reynolds number based on infinite-shear viscosity
$\langle Re\rangle$	Reynolds number based on the tank-averaged apparent viscosity
ss	(subscript) steady-state

REFERENCES

Amanullah, A., S. A. Hjorth and A. W. Nienow, "A New Mathematical Model to Predict Cavern Diameters in Highly Shear Thinning, Power Law Liquids Using Axial Flow Impellers," Chem. Eng. Sci. **53**, 455–469 (1998).

Arratia, P. E., J. Kukura, J. Lacombe and F. J. Muzzio, "Mixing of Shear-Thinning Fluids With Yield Stress in Stirred Tanks," AIChE J. **52**, 2310–2322 (2006).

Brostow, W., H. E. Hagg Lobland, T. Reddy, R. P. Singh and L. White, "Lowering Mechanical Degradation of Drag Reducers in Turbulent Flow," J. Mater. Res. **22**, 56–60 (2007).

Chen, S. and G. D. Doolen, "Lattice Boltzmann Method for Fluid Flows," Annu. Rev. Fluid Mech. **30**, 329–364 (1989).

Couerbea, G., D. F. Fletcher, C. Xuereb and M. Poux, "Impact of Thixotropy on Flow Patterns Induced in a Stirred Tank: Numerical and Experimental Studies," Chem. Eng. Res. Des. **86**, 545–553 (2008).

Derksen, J. J., "Scalar Mixing by Granular Particles," AIChE J. **54**, 1741–1747 (2008).

Derksen, J. J., "Solid Particle Mobility in Agitated Bingham Liquids," Ind. Eng. Chem. Res. **48**, 2266–2274 (2009).

Derksen, J. J. and Prashant. "Simulations of Complex Flow of Thixotropic Liquids," J. Non-Newton. Fluid Mech. **160**, 65–75 (2009).

Derksen, J. and H. E. A. Van den Akker, "Large-Eddy Simulations on the Flow Driven by a Rushton Turbine," AIChE J. **45**, 209–221 (1999).

Dullaert, K. and J. Mewis, "Thixotropy: Build-Up and Breakdown Curves During Flow," J. Rheol. **49**, 1213–1230 (2005).

Elson, T. P., "The Growth of Caverns Formed Around Rotating Impellers During the Mixing of a Yield Stress Fluid," Chem. Eng. Commun. **96**, 303–319 (1990).

Elson, T. P., D. J. Cheesman and A. W. Nienow, "X-Ray Studies of Cavern Sizes and Mixing Performance With Fluids Possessing a Yield Stress," Chem. Eng. Sci. **41**, 2555–2562 (1986).

Escudier, M. P., S. Rosa and R. J. Poole, "Asymmetry in Transitional Pipe Flow of Drag-Reducing Polymer Solutions," J. Non-Newton. Fluid Mech. **161**, 19–29 (2009).

Ferroir, T., H. T. Huynh, X. Chateau and P. Coussot, "Motion of a Solid Object Through a Pasty (Thixotropic) Fluid," Phys. Fluids **16**, 594–601 (2004).

Goldstein, D., R. Handler and L. Sirovich, "Modeling a No-Slip Flow Boundary With an External Force Field," J. Comp. Phys. **105**, 354–366 (1993).

Hartmann, H., J. J. Derksen and H. E. A. Van den Akker, "Mixing Times in a Turbulent Stirred Tank by Means of LES," AIChE J. **52**, 3696–3706 (2006).

Lucas, E. F., C. R. E. Mansur, L. Spinelli, and J. G. C. Queiros, "Polymer Science Applied to Petroleum Production," Pure & Appl. Chem. **81**, 473–494 (2009).

Masliyah, J., Z. J. Zhou, Z. Xu, J. Czarnecki and H. Hamza, "Understanding Water-Based Bitumen Extraction From Athabasca Oil Sands," **82**(4), 628–654 (2004).

Moore, F., "The Rheology of Ceramic Slips and Bodies," Trans. Br. Ceram. Soc. **58**, 470–494 (1959).

Mujumdar, A., A. N. Beris and A. B. Metzner, "Transient Phenomena in Thixotropic Systems," J. Non-Newton. Fluid Mech. **102**, 157–178 (2002).

Somers, J. A., "Direct Simulation of Fluid Flow With Cellular Automata and the Lattice-Boltzmann Equation," Appl. Sci. Res. **51**, 127–133 (1993).

Storey, B. T. and E. W. Merrill, "The Rheology of Aqueous Solution of Amylose and Amylopectine With Reference to Molecular Configuration and Intermolecular Association," J. Polym. Sci. **33**, 361–375 (1958).

Succi, S., "The Lattice Boltzmann Equation for Fluid Dynamics and Beyond," Clarendon Press, Oxford (2001).
Sweby, P. K., "High Resolution Schemes Using Flux Limiters for Hyperbolic Conservation Laws," SIAM J. Numer. Anal. **21**, 995–1011 (1984).
Tiljander, P., B. Ronnmark and H. Theliander, "Characterisation of Three Different Impellers Using the LDV-Technique," Can. J. Chem. Eng. **75**(4), 787–793 (1997).
Yu, D. Z., R. W. Mei, L. S. Luo and W. Shyy, "Viscous Flow Computations With the Method of Lattice Boltzmann Equation," Progr. Aerosp. Sci. **39**, 329–367 (2003).

Manuscript received January 25, 2010; revised manuscript received March 1, 2010; accepted for publication March 4, 2010.